molecular pharmaceutics

pubs.acs.org/molecularpharmaceutics

Article

Synthesis and Evaluation of ^{99m}Tc-Labeled $_D$Pro-Gly-Containing Tracers Targeting PSMA

Zuojie Li, Yuhao Jiang, Qing Ruan,* Guangxing Yin, Peiwen Han, Xiaojiang Duan, and Junbo Zhang*

Cite This: *Mol. Pharmaceutics* 2024, 21, 5305−5314

Read Online

ACCESS | Metrics & More | Article Recommendations | Supporting Information

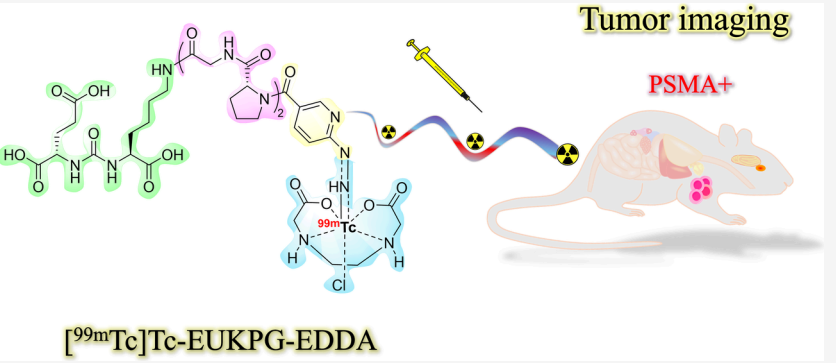

ABSTRACT: The specific expression of prostate-specific membrane antigen (PSMA) makes it an ideal target for the diagnosis and treatment of prostate cancer. Currently, many ^{99m}Tc-labeled PSMA-targeted tracers have been developed. However, the high renal uptake of these ^{99m}Tc-labeled tracers is a common problem that limits their clinical application. In this work, the ligand (EUKPG) using $_D$Pro-Gly as the linker was synthesized and three ^{99m}Tc-labeled complexes ([^{99m}Tc]Tc-EUKPG-EDDA, [^{99m}Tc]Tc-EUKPG-TPPTS, [^{99m}Tc]Tc-EUKPG-TPPMS) with different coligands were prepared and evaluated. Among them, [^{99m}Tc]Tc-EUKPG-EDDA showed the most favorable pharmacokinetic properties, with significantly reduced uptake in the kidney (14.04 ± 0.23% ID/g), rapid clearance and low uptake in nontarget organs, thus making it to exhibit high tumor-to-background ratios (tumor/blood: 7.47, tumor/muscle: 12.65). Affinity studies have shown that it has high specificity for PSMA both *in vivo* and *in vitro*. Therefore, [^{99m}Tc]Tc-EUKPG-EDDA has great potential as a promising molecular tracer to target PSMA for tumor imaging.

KEYWORDS: *PSMA, tracer, tumor, ^{99m}Tc, SPECT*

INTRODUCTION

The expression of prostate-specific membrane antigen (PSMA) in prostate epithelial cells of prostate cancer patients is 100 to 1000 times higher than that of normal people.[1,2] It is also expressed in the new blood vessels of solid tumors and is considered to be an ideal target for the diagnosis and treatment of prostate cancer.[3] In recent years, radiopharmaceuticals targeting PSMA have been rapidly developed in nuclear medicine imaging and treatment of tumors.[4−7]

Small molecule inhibitors containing glu-urea-lysine (EUK) specifically bind to PSMA on the surface of prostate cancer cells.[8] Radionuclide-labeled inhibitors containing EUK targeting PSMA have become the mainstream in international radiopharmaceutical research.[9,10] ^{99m}Tc is the best nuclide for single photon emission computed tomography (SPECT) imaging due to its ideal physical decay characteristics, convenient availability and rich coordination chemical properties.[11,12] Therefore, the development of new ^{99m}Tc-labeled tumor radiopharmaceuticals targeting PSMA has an important scientific and application values.

In the past decade, ^{99m}Tc-labeled PSMA tracers have been widely studied,[12−15] such as [^{99m}Tc]Tc-MIP-1404 with $[Tc(CO)_3]^+$ core,[16] [^{99m}Tc]Tc-PSMA-I&S with $[TcO]^{3+}$ core,[17] [^{99m}Tc]Tc-EDDA/HYNIC-iPSMA,[18] [^{99m}Tc]Tc-HYNIC-ALUG[19] and [^{99m}Tc]Tc-PSMA-T4[20] conjugated with hydrazinonicotinamide (HYNIC) bifunctional linker, which have entered the clinical research stage. Preliminary clinical results indicate that none is superior to positron emission tomography (PET) tracers, except for the inherent advantages of PET over SPECT.[14] Common problems in the diagnosis of prostate cancer include poor sensitivity compared to [^{68}Ga]Ga-PSMA-11 in detecting small, metastatic lesions and low prostate-specific antigen (PSA) concentrations, and

Received: July 20, 2024
Revised: September 11, 2024
Accepted: September 11, 2024
Published: September 19, 2024

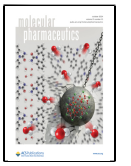

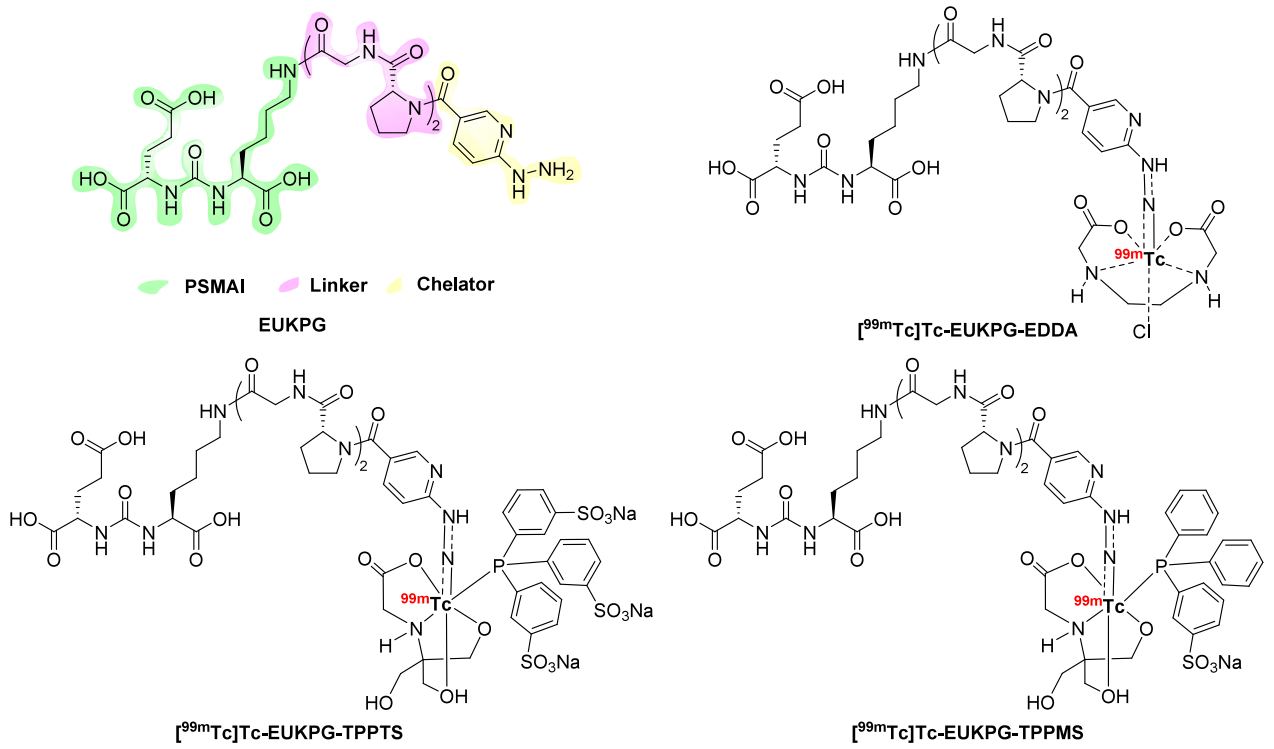

Figure 1. Structures of EUKPG and ^{99m}Tc-labeled EUKPG radiotracers.

high accumulation in the kidneys and renal excretion, which can make image interpretation difficult.[4,5,14,21] Improving the absolute uptake in tumors and reducing the high accumulation in kidneys to further improve the tumor-to-kidney ratio of the tracer may be a potential strategy for optimizing the pharmacokinetic properties of PSMA tracers in the future.

In ^{99m}Tc-labeled radiotracers, the linker between the targeting group and the nuclide chelator plays an important role in improving the pharmacokinetic properties. Akizawa et al.[22] studied the pharmacokinetic effects of $_D$Pro-Gly (PG) peptide as a linker in poly-RGD. Adjusting the length of the PG chains has a significant positive effect on improving the affinity of the tracer for integrin $\alpha_v\beta_3$, increasing the tumor-to-background ratios (TBRs) and the tumor retentions rate. At the same time, our research group also observed the same phenomenon when introducing oligopeptide chain $(PG)_2$ into the ^{99m}Tc-labeled fibroblast activation protein (FAP) tracers, especially in reducing uptake in nontarget organs.[23,24] As for ^{99m}Tc labeling, HYNIC as a common bifunctional linker, is one of the current research hotspots of ^{99m}Tc radiopharmaceuticals in recent years.[11,25−27] Since the HYNIC group contains only one coordinating atom, stable [^{99m}Tc]Tc-HYNIC complexes requires the participation of coligands such as triphenylphosphine trisulfonate (TPPTS), diphenylphosphine benzene-3-sulfonate (TPPMS), ethylenediaminediacetic acid (EDDA), and trimethylglycine (tricine). The rich composition and proportion of coligands can adjust the stability of the tracer, lipid solubility, and binding ability to target.[28,29] It is also the most commonly used chelators for ^{99m}Tc labeling PSMA tracers in the clinical.

Therefore, in this study, in order to improve the TBRs and decrease the uptake of kidney of PSMA tracers, we designed and synthesized the radioligand EUKPG (Figure 1) by using HYNIC as a chelator, $(PG)_2$ as a linker and EUK as a targeted group. By introducing different coligands (EDDA/tricine, TPPTS/tricine, and TPPMS/tricine), three different ^{99m}Tc-labeled PSMA tracers were prepared, and their pharmacokinetic properties and potential as SPECT imaging agents were evaluated *in vitro* and *in vivo*.

EXPERIMENTAL SECTION

Materials. All reactions were carried out under an atmosphere of nitrogen in flame-dried glassware with magnetic stirring unless otherwise indicated. All reagents were purchased from Aladdin, J&K, Innochem, Tong guang fine chemicals Company (Beijing, China). ^{1}H nuclear magnetic resonance (NMR) spectra were recorded on a 400 or 600 MHz JNM-ECS spectrometer (JEOL, Tokyo, Japan).The NMR chemical shifts were referenced to residual solvent peaks or to TMS as an internal standard. All coupling constants J were quoted in Hz. Mass spectra (MS) were obtained on a Thermo Scientific LCQ (Thermo, USA) mass spectrometer with ESI ionization.The radioactive high-performance liquid chromatography (R-HPLC) analyses were performed on a Shimadzu 20A (Shimadzu, Kyoto, Japan) equipped with a Kromasil C18 column (250 × 4.6 mm, 5 μm). [^{99m}Tc]$NaTcO_4$ was eluted with saline solution through a ^{99m}Mo/^{99m}Tc generator obtained from Zhibo Bio-Medical Tech (Beijing, China). Radioactivity was assessed using a HRS-1000 technetium analyzer (Huaruison, Beijing, China) and a Wizard 2480 γ-counter (PerkinElmer, Singapore). The 22Rv1 and PC3 cell lines were obtained from the Chinese Academy of Sciences Typical Culture Collection (Beijing, China). *In vivo* Imaging studies were performed on a micro-SPECT/CT device (Trifoil, CA, USA).

Chemical Synthesis and Radiosynthesis. *Preparation of Compound 2.* Compound **1** (2.0 g, 12.7 mmol) was dissolved in 20 mL of ethanol, and hydrazine hydrate (1.48 mL, 31.7 mmol) was added. The mixture was refluxed overnight and then cooled to room temperature to afford a

https://doi.org/10.1021/acs.molpharmaceut.4c00799
Mol. Pharmaceutics 2024, 21, 5305−5314

solid, which was collected by filtration and washed with petroleum ether/ethyl acetate (v/v = 2/1) to afford a yellow solid, identified as compound **2** (1.60 g, 81.0%). ^{1}H NMR (600 MHz, DMSO-d_6) δ 8.48 (d, J = 2.3 Hz, 1H), 7.81 (s, 1H), 6.67 (d, J = 8.9 Hz, 1H). MS-ESI: calcd for $[M + H]^+$: 154 (M = $C_6H_7N_3O_2$), found: 154.

Preparation of Compound ***3***. Compound **2** (2.0 g, 13.23 mmol) and di*tert*-butyl dicarbonate (3.18 g, 14.59 mmol) were dissolved in 10 mL of dimethylformamide (DMF). Triethylamine (TEA, 2.76 mL, 19.93 mmol) was subsequently added, and the mixture was stirred at room temperature for 12 h. The reaction progress was monitored by thin-layer chromatography (TLC), and the filtrate was concentrated. The residue was then purified by column chromatography using [DCM/MeOH = 50/1 (v/v)] to afford a white solid, identified as compound **3** (2.5 g, 74.5%). ^{1}H NMR (600 MHz, Methanol-d_4) δ 8.77 (d, J = 0.8 Hz, 1H), 8.20 (d, J = 8.8 Hz, 1H), 6.81 (d, J = 8.8 Hz, 1H), 1.42 (s, 9H). MS-ESI: calcd for [M]: 253 (M = $C_{11}H_{15}N_3O_4$), found: 253.

Preparation of Compound ***4***. Compound **3** (0.5 g, 1.97 mmol), ($_D$Pro-Gly)$_2$ (0.771 g, 2.36 mmol), and HATU (0.824 g, 2.17 mmol) were combined in a 25 mL reaction vessel. Five mL of DMF were then added to dissolve the contents of the bottle. TEA (0.41 mL, 2.96 mmol) was subsequently added, and the mixture was allowed to react at ambient temperature for 12 h. After the reaction was complete, the mixture was cooled to room temperature, and the solvent was removed under reduced pressure. The residue was then purified by column chromatography using [DCM/MeOH = 40/1 (v/v)] to afford a white solid, identified as compound **4** (0.58 g, 52.3%). ^{1}H NMR (600 MHz, Methanol-d_4) δ 8.48 (s, 1H), 8.02 (d, J = 8.8 Hz, 1H), 6.87 (d, J = 8.8 Hz, 1H), 4.65 (d, J = 88.5 Hz, 2H), 4.29−3.61 (m, 7H), 3.15 (d, J = 7.3 Hz, 1H), 2.48−1.95 (m, 8H), 1.66−1.37 (m, 9H). MS-ESI: calcd for $[M + Na]^+$: 584 (M = $C_{25}H_{35}N_7O_8$), found: 584.

Preparation of Compound ***6***. Triphosgene (2.0 g, 6.74 mmol) was dissolved into 20 mL of DCM, and then compound **5** (5.98 g, 20.22 mmol) and TEA (9.37 mL, 67.4 mmol) were added, stirred at room temperature for 1 h, and then N-E-benzyloxycarbonyl-L-lysine *tert*-butyl ester hydrochloride (7.54 g, 20.22 mmol) and TEA (2.81 mL, 20.22 mmol) were added, and reacted at room temperature for 2 h. After the reaction was completed, the solvent was distilled off under reduced pressure, and purified by column chromatography [DCM/MeOH = 100/1 (v/v)] to afford an oily substance, identified as compound **6** (8 g, 64.0%). ^{1}H NMR (600 MHz, DMSO-d_6) δ 7.42−7.18 (m, 5H), 6.27 (d, J = 23.8 Hz, 2H), 4.07−3.91 (m, 2H), 2.98 (d, J = 6.3 Hz, 2H), 2.22 (d, J = 16.8 Hz, 2H), 1.87 (d, J = 6.8 Hz, 1H), 1.67 (s, 3H), 1.45−1.35 (m, 27H), 1.30−1.15 (m, 3H), 0.86 (s, 1H). MS-ESI: calcd for $[M + H]^+$: 622 (M = $C_{32}H_{51}N_3O_9$), found: 622.

Preparation of Compound ***7***. Compound **6** (3.0 g, 4.82 mmol) was dissolved in 5 mL of methanol, followed by the addition of palladium carbon (340 mg, 0.174 mmol). The resulting mixture was allowed to react at room temperature under a hydrogen atmosphere for 12 h, with the reaction progress monitored by TLC. After the reaction was complete, the mixture was filtered through diatomaceous earth, and the solvent was subsequently removed under reduced pressure. The residue was then purified by column chromatography using [DCM/MeOH = 30/1 (v/v)] to afford an oily substance, identified as compound 7 (2.0 g, 85.0%). ^{1}H NMR (600 MHz, Chloroform-d) δ 5.20 (s, 1H), 4.34 (d, J = 5.0 Hz, 2H), 4.12 (d, J = 7.2 Hz, 1H), 2.68 (d, J = 1.3 Hz, 1H), 2.33 (d, J = 9.7 Hz, 2H), 2.05 (s, 2H), 1.81 (d, J = 5.8 Hz, 2H), 1.60 (s, 2H), 1.45 (d, J = 16.6 Hz, 27H), 1.26 (s, 2H). MS-ESI: calcd for $[M + H]^+$: 488 (M = $C_{24}H_{45}N_3O_7$), found: 488.

Preparation of Compound ***8***. Compound **4** (100 mg, 0.178 mmol), HATU (74.50 mg, 0.196 mmol), and compound **7** (130.20 mg, 0.267 mmol) were combined in a 25 mL reaction vessel. To this mixture, 5 mL of DMF was added to dissolve the reactants, followed by the introduction of TEA (37 μL, 0.267 mmol). The reaction mixture was allowed to proceed at room temperature for 12 h, with the progress of the reaction being monitored via TLC. After the reaction was complete, the mixture was cooled to room temperature, and the solvent was removed under reduced pressure. The resulting residue was then purified by column chromatography using [DCM/MeOH = 60/1 (v/v)] to yield a colorless oil, identified as compound **8** (0.15 g, 64.5%). ^{1}H NMR (600 MHz, Methanol-d_4) δ 8.71 (d, J = 2.3 Hz, 1H), 8.17 (s, 1H), 6.88 (s, 1H), 4.33 (m, J = 23.4 Hz, 2H), 3.56−3.51 (m, 2H), 3.48 (p, J = 1.7 Hz, 1H), 3.16 (d, J = 6.5 Hz, 1H), 2.48 (s, 2H), 2.21 (s, 1H), 1.96 (d, J = 14.2 Hz, 2H), 1.81 (d, J = 7.3 Hz, 4H), 1.72−1.55 (m, 41H), 1.49 (s, 2H). MS-ESI: calcd for $[M + Na]^+$: 1053 (M = $C_{49}H_{78}N_{10}O_{14}$), found: 1053.

Preparation of EUKPG. Compound **8** (100 mg, 0.97 mmol) was dissolved in 2 mL of DCM. To this solution, 2 mL of trifluoroacetic acid (TFA) was added, and the resulting mixture was allowed to react at room temperature for 3 h. The reaction progress was monitored using TLC. After the reaction was complete, the reaction mixture was cooled to room temperature. The solvent was removed under reduced pressure, leaving behind a residue. The resulting residue was then purified by column chromatography using [DCM/MeOH = 5/1 (v/v)] to yield a colorless oil, identified as **EUKPG** (60 mg, 81.8%). ^{1}H NMR (400 MHz, Methanol-d_4) δ 8.55 (d, J = 43.3 Hz, 1H), 8.26 (s, 1H), 7.06 (d, J = 9.3 Hz, 1H), 4.36 (d, J = 4.7 Hz, 2H), 3.76 (d, J = 16.0 Hz, 3H), 3.42 (d, J = 27.0 Hz, 8H), 3.06 (s, 1H), 2.49 (s, 2H), 2.09 (d, J = 105.5 Hz, 4H), 1.74 (s, 4H), 1.64−1.31 (m, 7H). MS-ESI: calcd for $[M-H]^-$: 761(M = $C_{32}H_{46}N_{10}O_{12}$), found: 761.

Preparation of [^{99m}Tc]Tc-EUKPG-TPPTS. Tricine (1 mg) and TPPTS (2 mg) were dissolved in 0.5 mL of phosphate buffered saline (PBS). To this solution, succinate buffer adjusted to a pH of 5.0 was added, followed by EUKPG (10 μg) and 0.5 mL of freshly eluted [^{99m}Tc]$NaTcO_4$ (37−370 MBq) in sequence, and the mixture was then subjected to a reaction at 100 °C for 30 min to yield the radiotracer [^{99m}Tc]Tc-EUKPG-TPPTS.

Preparation of [^{99m}Tc]Tc-EUKPG-TPPMS. Tricine (1 mg) and TPPMS (2 mg) were dissolved in 0.5 mL of PBS. To this solution, succinate buffer adjusted to a pH of 5.0 was added, followed by EUKPG (10 μg) and 0.5 mL of freshly eluted [^{99m}Tc]$NaTcO_4$ (37−370 MBq) in sequence, and the mixture was then subjected to a reaction at 100 °C for 30 min to yield the radiotracer [^{99m}Tc]Tc-EUKPG-TPPMS.

Preparation of [^{99m}Tc]Tc-EUKPG-EDDA. Tricine (20 mg) and EDDA (10 mg) were dissolved in 0.5 mL of PBS. To this solution, succinate buffer adjusted to a pH of 7.0 was added, adjust the solution pH to 7.0−8.0 with NaOH (1 mol/L), followed by EUKPG (10 μg), $SnCl_2{\cdot}2H_2O$(100 μg) and 0.5 mL of freshly eluted [^{99m}Tc]$NaTcO_4$ (37−370 MBq) in sequence, and the mixture was then subjected to a reaction at

https://doi.org/10.1021/acs.molpharmaceut.4c00799
Mol. Pharmaceutics 2024, 21, 5305−5314

100 °C for 20 min to yield the radiotracer [^{99m}Tc]Tc-EUKPG-EDDA.

All ^{99m}Tc-labeled complexes do not require purification, with a radiochemical purity (RCP) of >90%.

R-HPLC Analysis and Stability Assay. The RCP and stability of the ^{99m}Tc label complexes were determined by R-HPLC. R-HPLC analysis was performed on a Shimadzu 20A equipped with a Kromasil C18 column (250 × 4.6 mm, 5 μm). The injection volume was 10 μL. The flow rate was 1.0 mL min^{-1}. Phase A was water containing 0.1% TFA, while phase B was acetonitrile. The flow rate was 1.0 mL/min. The R-HPLC program was as follows: 10% phase B (stationary from 0 to 2 min); 10% to 90% phase B (linear increase from 2 to 5 min); 90% phase B (stationary time 5 to 20 min); 90% to 10% phase B (linear decrease from 20 to 25 min).

In vitro stability was evaluated in saline and mice whole blood. The radiolabeled solution was stored at 37 °C for 4 h and then RCP was determined by R-HPLC. To evaluate the whole blood stability, radiolabeled EUKPG was incubated with fresh mice blood in equal proportions (v/v) at 37 °C for 4 h to measure the whole blood stability. Then, a solvent mixture of acetonitrile and ethanol (v/v = 1:1) was added to the incubated mixture in a ratio of 1:2 (v/v) and centrifuged at 12000 rpm for 5 min (4 °C) to pellet plasma proteins. Then, the supernatant was filtered with a 0.22 μm filter membrane and analyzed by R-HPLC to evaluate the RCP.

Octanol/Water Partition Coefficient (Log *P*). Log *P* values of the three radiotracers were tested by shake flask method. The *n*-octanol used in the experiment was presaturated with PBS (0.025 mol/L, pH 7.4) overnight. Briefly, 100 μL of radiotracer, 1 mL of *n*-octanol, and 900 μL of PBS were added to a centrifuge tube, and the mixture was shaken vigorously for 5 min. After that, the mixture was centrifuged at 10000 rpm for 5 min to achieve phase separation. Samples of 100 μL of *n*-octanol and PBS were collected and analyzed by γ-counter. The partition coefficient was obtained by comparing the radioactivity counts in the two phases. The results were based on three parallel experiments, calculated as log *P* = log (cpm in *n*-octanol/cpm in PBS), and log *P* values were expressed as mean ± SD.

Cell Culture and Tumor Models. Cancer cell lines 22Rv1 (PSMA+) and PC3 (PSMA-) were cultured in DMEM with 10% (v/v) heat-inactivated FBS (fetal bovine serum) and 1% (v/v) penicillin-streptomycin at 37 °C in a cell culture incubator with 5% CO_2.

All mice were purchased from Shibeifu Experimental Animal Company (Beijing, China). All mice had access to food and water ad libitum with a 12:12 h light cycle and were maintained under temperature-control (23 ± 2 °C). Male Kunming mice (4 weeks old) were used for preliminary pharmacokinetic studies. Murine 22Rv1 or PC3 cells (approximately 1 × 10^7) suspended in PBS (100 μL) were injected subcutaneously into the flank of male BALB/c nude mice (4 weeks old), and 2 weeks later (tumor diameter was approximately 5−10 mm), biodistribution and SPECT imaging were evaluated in the 22Rv1 and PC3 mice model.

Biodistribution Studies in Mice. For the preliminary pharmacokinetic study of the three radiotracers, evaluation was performed in Kunming mice (4 weeks old) (n= 5), and each mouse was injected with ^{99m}Tc-labeled tracer (1.85 ± 0.05 MBq, 100 μL) via the tail vein and sacrificed at 2 h after injection. Blood and other major organs (heart, liver, spleen, lung, kidney, muscle, bone, stomach, brain, large intestine and small intestine) were collected, weighed, and counted using γ-counter. In the blocking study, mice were preinjected with PSMA-selective inhibitor 2-PMPA (500 μg, 100 μL) 30 min in advance, followed by intravenous injection of ^{99m}Tc-labeled tracer (1.85 ± 0.05 MBq, 100 μL), and sacrificed at 2 h after injection. The biodistribution study in the 22Rv1 mice model (n= 3) was the same as above, and the data obtained were expressed as the percentage of injected dose uptake per gram of organ or tissue (%ID/g), and the values were shown as mean ± SD.

Cellular Uptake and Saturation Binding Assay *In Vitro*. 22Rv1 and PC3 cells were seeded in 24-well plates (1 × 10^5 cells per well) and incubated overnight. [^{99m}Tc]Tc-EUKPG-EDDA (0.37 MBq,) in 0.5 mL of fresh culture medium was added to each well. The culture medium was removed after 1h and 2 h, respectively, and the cells were washed twice with cold PBS and lysed with NaOH (1M). Radioactivity was measured using a γ-counter. For the blocking experiment, the PSMA inhibitor 2-PMPA (1 μM) was used for intervention 30 min in advance, and the subsequent operation method was the same as the experimental group. The results are expressed as the percentage of injected activity (IA %)/10^5 cells compared to the 22Rv1 control group, and the values were shown as mean ± SD.

Saturation binding assays were performed as described in the literature.[30] Different concentrations of [^{99m}Tc]Tc-EUKPG-EDDA (1.56−1000 nM) were added to 22Rv1 cells in 96-well plates, intervention was performed 30 min in advance in the inhibition group (500 nM per well). After incubation for 1 h, the medium was removed, the cells were washed twice with cold PBS, lysed with NaOH (1M), and the radioactivity was measured by γ-counter. The results are expressed as the percentage of specific binding (SB %)/10^5 cells. The data obtained were used to calculate the dissociation constant (K_d) by GraphPad Prism 8.2 to determine the affinity for PSMA.

Small Animal Micro-SPECT/CT Imaging. [^{99m}Tc]Tc-EUKPG-EDDA (37 MBq, 100 μL,) was injected intravenously into 22Rv1 or PC3 mice models (n= 2). Mice were first anesthetized with 3% (v/v) isoflurane and SPECT/CT images were acquired by static scanning 2 and 4 h after injection with 1.5% isoflurane in air at 500 mL/min. Blockade studies were performed in mice bearing 22Rv1 tumors by preinjection of 2-PMPA (500 μg) via the tail vein 30 min in advance, followed by injection of 100 μL [^{99m}Tc]Tc-EUKPG-EDDA (37 MBq). Under the same conditions, anesthesia blocking group mice and collect images after injection 2 h.

Molecular Docking and Dynamics Assay. Molecular docking was performed in the workspace of Auto Dock 4.2. The protein crystal structure (PDB: 4LQG) downloaded from the Protein Data Bank (PDB) was used as the docking receptor. Tc-EUKPG-EDDA was used for docking simulations using the Amber 99 force field in the Gaussian 09 workspace for 3D structure optimization. The cocrystallized ligand was used as the docking center, and no restrictions were imposed in the default settings when defining the binding sites for subsequent docking studies. The preliminary docking results were subjected to molecular dynamics in Gromacs 2020, using the GAFF atomic model for small molecule optimization, the Amber 99 stand for protein structure optimization, the SPC for the water model, the NVT and NPT pre-equilibration for 2 ns, and the dynamic simulation time for 50 ns. The molecular dynamics results were analyzed for root-mean-square fluctuation (RMSF) and root-mean-square deviation (RMSD), and

https://doi.org/10.1021/acs.molpharmaceut.4c00799
Mol. Pharmaceutics 2024, 21, 5305−5314

Scheme 1. Synthetic Route of EUKPG[a]

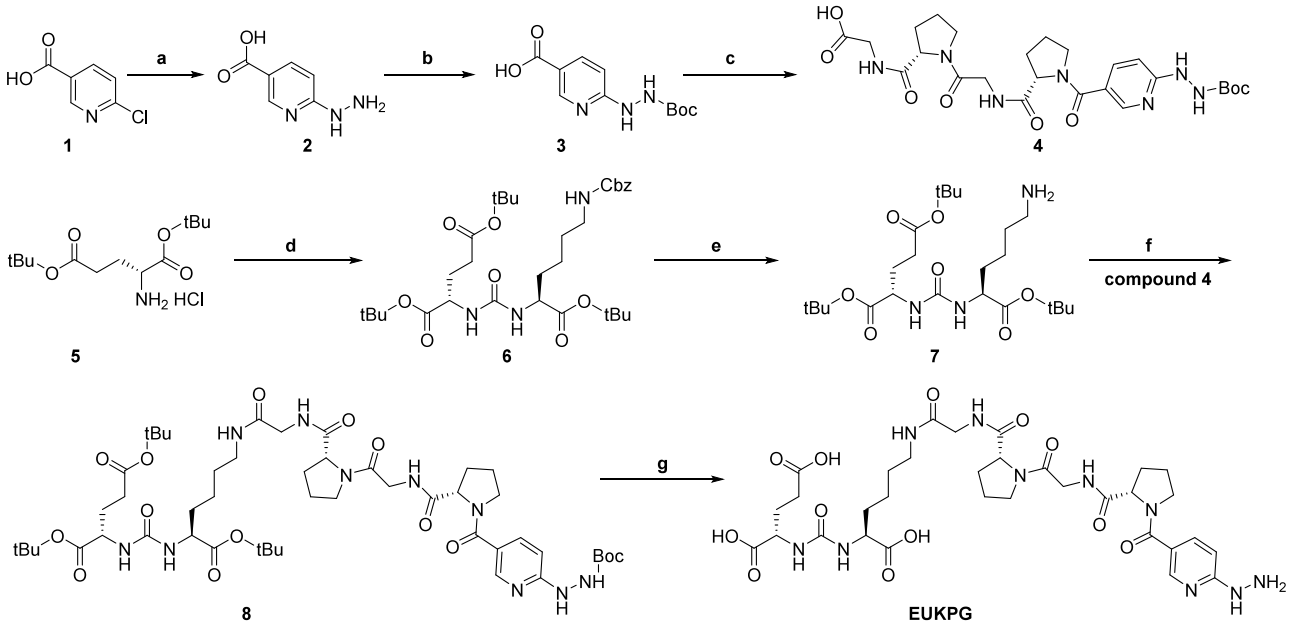

[a](a) Hydrazine hydrate, EtOH, 100 °C, 4 h; (b) Di-*tert*-butyl dicarbonate, TEA, DMF, rt, 12 h; (c) $(_{D}Pro\text{-}Gly)_2$, HATU, TEA, DMF, rt, 3 h; (d) Triphosgene, H-Lys(Z)-OtBu.HCl, TEA, DCM, rt,12 h; (e) Pd/C, H_2, MeOH, rt,12 h; (f) HATU, TEA,DMF, rt, 12 h; (g) TFA, DCM, rt, 3 h.

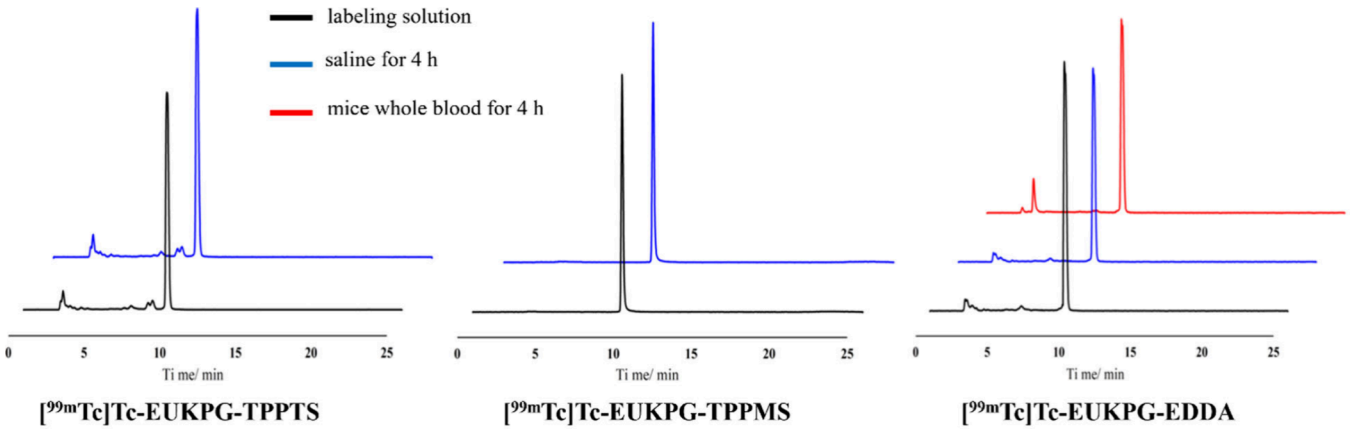

Figure 2. Stability of three ^{99m}Tc-labeled EUKPG radiotracers in saline or whole blood of mice.

the molecular mechanicspoisson-boltzmann surface area (MMPBSA) energy calculation was performed for the last 10 ns, and the energy results were decomposed. The last frame of the simulation results was output as the final conformation, which was visualized and analyzed in PyMOL.

Statistical Analysis. Statistical analysis was performed using a 2-tailed *t* test. P values were considered significant if they were less than 0.05.

RESULTS

Chemistry and Radiochemistry. The synthesis of EUKPG labeled precursors is shown in Scheme 1, and the structures of all compounds were confirmed by ^{1}H NMR and MS. Three ^{99m}Tc-labeled EUKPG tracers were prepared by different coligand combinations, R-HPLC chromatograms (black line in Figure 2) and the inferred structures are shown in Figure 1. The RCP is above 90%, and they can be used directly without purification. The molar activities of the three radiotracers were 2.82 × 10^7 Bq/mol. The retention times (RT) of [^{99m}Tc]Tc-EUKPG-TPPTS, [^{99m}Tc]Tc-EUKPG-TPPMS and [^{99m}Tc]Tc-EUKPG-EDDA were 9.48, 9.46, and 9.39 min, respectively.

Stability and Log *P* Assessment. As shown in Figure 2, the three ^{99m}Tc-labeled EUKPG tracers showed good *in vitro* stability after incubation in saline (blue line) at 37 °C for 4 h, and [^{99m}Tc]Tc-EUKPG-EDDA showed negligible decomposition (approximately 3.5%) in mice whole blood (red line) at 37 °C, indicating that they are stable under physiological conditions. [^{99m}Tc]Tc-EUKPG-TPPTS, [^{99m}Tc]Tc-EUKPG-TPPMS and [^{99m}Tc]Tc-EUKPG-EDDA are all hydrophilic tracers with Log *P* of −1.05 ± 0.07, −0.39 ± 0.01 and −1.32 ± 0.02, respectively.

Biodistribution Studies. Pharmacokinetic studies of three ^{99m}Tc-labeled EUKPG tracers in normal Kunming mice are shown in Figure 3 A and Table S1. The uptake in the blood was all below 1% ID/g at 2 h after injection, and all showed low uptake in nonmetabolizing organs. In addition to the high uptake of [^{99m}Tc]Tc-EUKPG-TPPMS in the large intestine

https://doi.org/10.1021/acs.molpharmaceut.4c00799
Mol. Pharmaceutics 2024, 21, 5305−5314

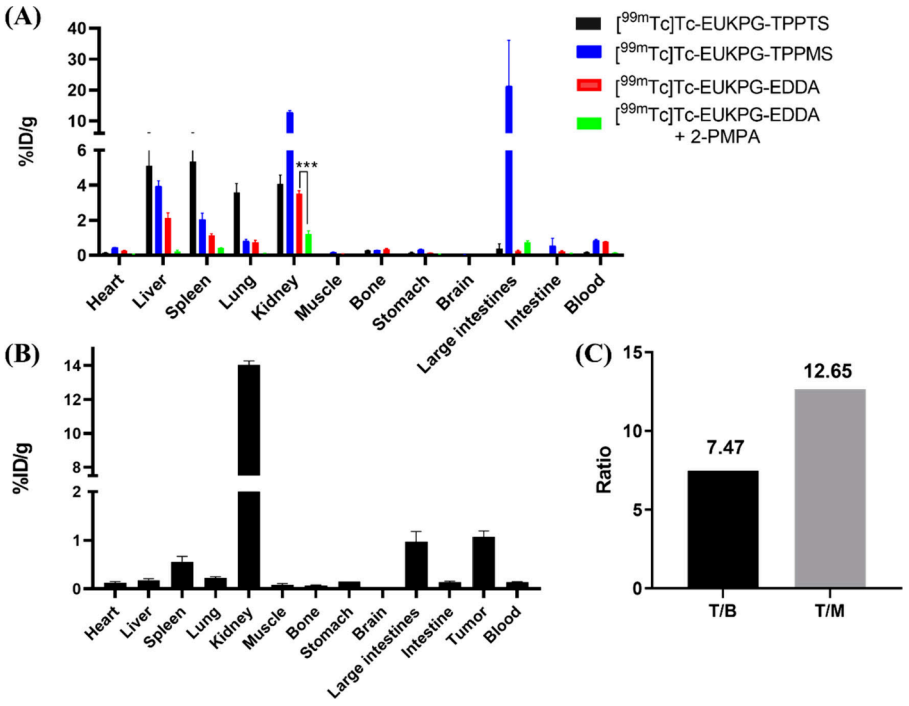

Figure 3. Biodistribution of three ^{99m}Tc-labeled EUKPG radiotracers in mice. (A) Biodistribution of normal Kunming mice (n = 5) at 2 h after injection, (B) [^{99m}Tc]Tc-EUKPG-EDDA biodistribution of 22Rv1 tumor-bearing mice (n = 3) at 2 h after injection, and (C) ratio of tumor-to-nontarget tissue in 22Rv1 tumor-bearing mice (T/B = tumor/Blood, T/M = tumor/muscle). *P < 0.05, **P < 0.01, ***P < 0.001.

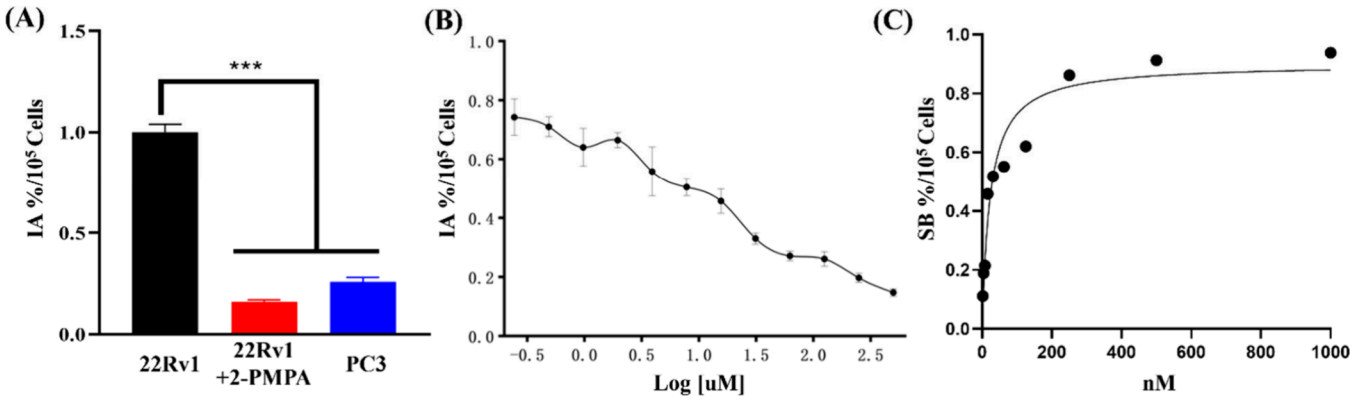

Figure 4. (A) Uptake of [^{99m}Tc]Tc-EUKPG-EDDA in 22Rv1 (PSMA+) and PC3 (PSMA-) cells. (B) Effects of different concentrations of blockers on the uptake of [^{99m}Tc]Tc-EUKPG-EDDA in 22Rv1 cells. (C) Saturation binding experiments of [^{99m}Tc]Tc-EUKPG-EDDA in 22Rv1 cells. *P < 0.05, **P < 0.01, ***P < 0.001.

(21.20 ± 14.92%ID/g), the uptake by the kidneys is the highest among all metabolic organs. Compared to [^{99m}Tc]Tc-EUKPG-TPPTS and [^{99m}Tc]Tc-EUKPG-TPPMS, [^{99m}Tc]Tc-EUKPG-EDDA has the lowest renal uptake (3.51 ± 0.18% ID/g), also has the advantage of low uptake in organs such as the heart, liver, spleen, and lung. In the case of preinjection of 2-PMPA blocker, the uptake of [^{99m}Tc]Tc-EUKPG-EDDA in the kidneys was significantly reduced (3.51 ± 0.18% ID/g vs 1.23 ± 0.17% ID/g).

The distribution of [^{99m}Tc]Tc-EUKPG-EDDA in 22Rv1 mice model is shown in Figure 3 B and Table S2. The uptake in the kidney (14.04 ± 0.23% ID/g) was the highest among the tissues of interest, followed by the tumor (1.07 ± 0.12% ID/g). Excitingly, the uptake in other nontarget organs is less than 1% ID/g. As shown in Figure 3 C, lower nontarget uptake resulted in high TBRs (T/B = 7.47, T/M = 12.65).

Cellular Uptake Studies. [^{99m}Tc]Tc-EUKPG-EDDA showed differential uptake in 22Rv1 (PSMA+) and PC3 (PSMA-) cells (Figure 4 A). Compared with 22Rv1 cells, the uptake in PC3 cells was reduced by 74%. At the same time, in the presence of the blocker 2-PMPA (1 μM), the inhibition rate of cell uptake was as high as 84%. Both have demonstrated that [^{99m}Tc]Tc-EUKPG-EDDA exhibits PSMA-dependent uptake in cells, verifying its effective targeting of PSMA. In addition, intervention with different concentrations of blockers (Figure 4 B) showed that the cellular uptake of [^{99m}Tc]Tc-EUKPG-EDDA was negatively correlated with the concentration of competitive blockers, further proving its specific binding to PSMA. Saturation binding experiments (Figure 4 C) showed that [^{99m}Tc]Tc-EUKPG-EDDA had a high nanomolar affinity (K_d = 23.33 nM) for PSMA.

Micro-SPECT/CT Imaging Studies. Micro-SPECT/CT imaging showed that [^{99m}Tc]Tc-EUKPG-EDDA had clear

https://doi.org/10.1021/acs.molpharmaceut.4c00799
Mol. Pharmaceutics 2024, 21, 5305−5314

tumor uptake in the 22Rv1 mice model (Figure 5 A), and low uptake in other organs except the kidney and intestine,

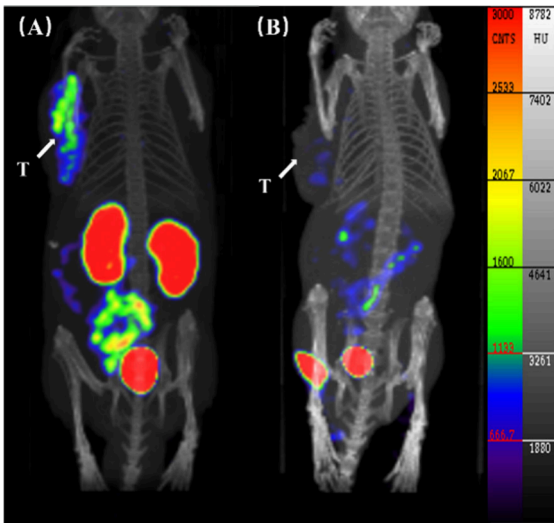

Figure 5. Micro-SPECT/CT images of [^{99m}Tc]Tc-EUKPG-EDDA (A, control; B, blocked by 2-PMPA) at 2 h after injection in 22Rv1 tumor-bearing BALB/c male nude mice.

indicating that the tracer has the potential for diagnosis of PSMA-related diseases. Preinjection of the blocking agent 2-PMPA effectively reduced its uptake in the kidney and tumor (Figure 5 B). Meanwhile, in the PC3 mice model (Figure S1), tumor uptake was almost negligible, while uptake in the kidney was still obvious, demonstrating the efficient targeting properties of [^{99m}Tc]Tc-EUKPG-EDDA to PSMA. In addition, SPECT/CT imaging at different time points showed that tumors could be clearly identified within 2 to 4 h (Figure S1).

Molecular Dynamics and Docking Studies. MD simulation results show that Tc-EUKPG-EDDA can form extensive hydrogen bonds and hydrophobic interactions in the active cavity of the protein (4LQG) (Figure 6 A). The RMSD (Figure 6 B) of the protein skeleton and protein−ligand indicates the stability of the entire 50 ns simulation system and the reliability of the simulation results analysis. The RMSF (Figure 6 C) and local flexibility analysis of Tc-EUKPG-EDDA show that the ligand residues fluctuate significantly, further indicating that the ligand is tightly bound to the active cavity of the protein. MMPBSA energy calculation shows that the total energy of the system dG = −36.034 kJ/mol, and the theoretical affinity between the ligand and the protein calculated by the total energy is at the nanomolar level (approximately 100 nM).The energy decomposition results showed (Figure 6 D) that the binding free energy dH = −127.834 kJ/mol (including molecular mechanics energy (MM) = −924.668 kJ/mol, polarized solvation energy (PB) = 836.371 kJ/mol, nonpolar solvation energy (SA) = −39.537 kJ/mol). As shown in Figure 6 E, ARG534 and GLU542 are the main residues contributing to the energy.

DISCUSSION

In this study, we conjugated the PSMA targeting group EUK with the bifunctional linker HYNIC through the $(PG)_2$ chain, designed and synthesized the labeling precursor EUKPG. Since ^{99m}Tc is the best nuclide for SPECT imaging (suitable half-life, rich coordination valence state and convenient and low-cost source), it aroused our strong interest. Three ^{99m}Tc-labeled PSMA tracers containing different coligands were prepared. The RCP of [^{99m}Tc]Tc-EUKPG-TPPTS, [^{99m}Tc]Tc-EUKPG-TPPMS, and [^{99m}Tc]Tc-EUKPG-EDDA are more than 90%, and can be used directly without purification. The labeling method is simple and convenient, which facilitates its subsequent application in research.

Stability studies showed that no obvious decomposition or dissociation was detected for the three ^{99m}Tc-labeled EUKPG tracers in normal saline for 4 h. Among them, [^{99m}Tc]Tc-

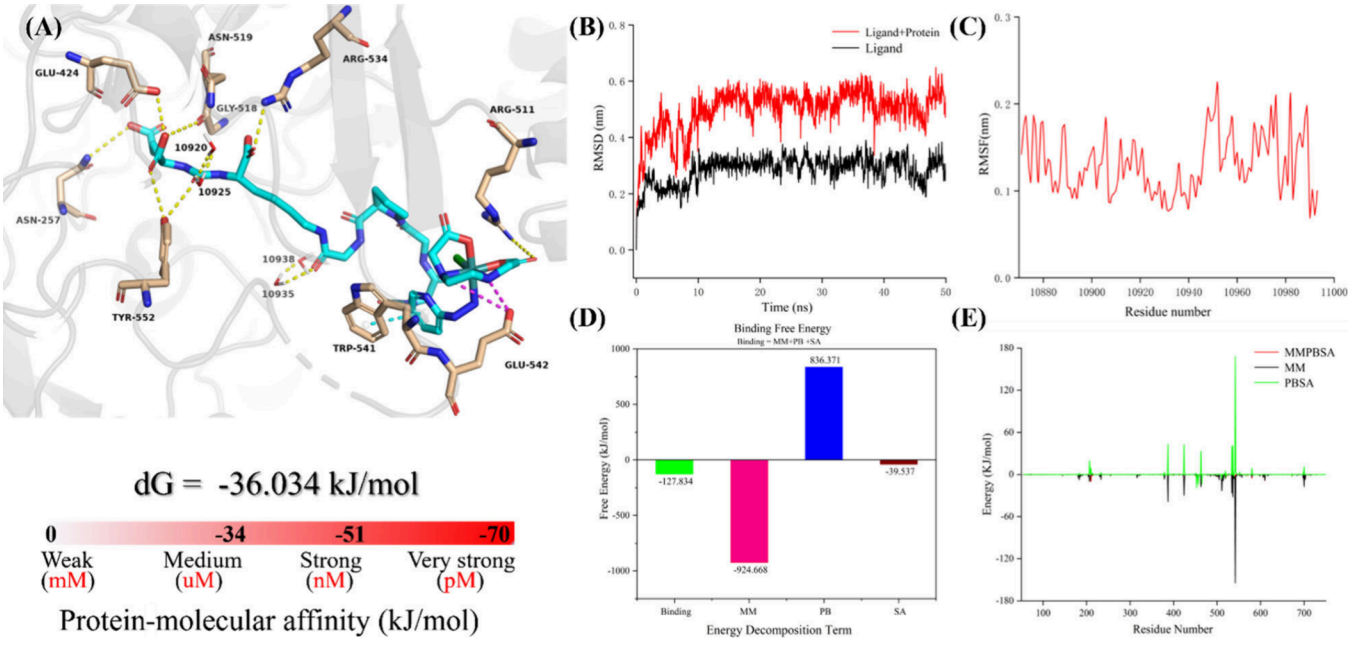

Figure 6. Molecular dynamics of Tc-EUKPG-EDDA. (A) Interactions within protein cavities; (B) ligands and ligand-protein RMSD; (C) ligands RMSF; (D) MMPBSA energy breakdown; and (E) contribution of protein residues to MMPBSA energy.

https://doi.org/10.1021/acs.molpharmaceut.4c00799
Mol. Pharmaceutics 2024, 21, 5305−5314

EUKPG-EDDA was observed to decompose slightly (RT = 3.26 min) in mice whole blood at 37 °C for 4 h, but its RCP was still higher than 90%, indicating that they have good *in vitro* stability. All three tracers are hydrophilic substances. Compared with [^{99m}Tc]Tc-EUKPG-TPPMS (Log *P*= −0.39 ± 0.01), [^{99m}Tc]Tc-EUKPG-TPPTS, and [^{99m}Tc]Tc-EUKPG-EDDA have lower Log *P*, which are −1.05 ± 0.07 and −1.32 ± 0.02, respectively. This indicates that the coligand plays a key role in regulating the lipid−water distribution of the tracer. For the above three tracers, the order of the three coligands in regulating hydrophilicity is EDDA/tricine > TPPTS/tricine > TPPMS/tricine.

A preliminary evaluation of the pharmacokinetics of three ^{99m}Tc-labeled PSMA tracers was conducted in normal Kunming mice in order to screen promising tracers for subsequent in-depth research. The uptake of the three tracers into blood, muscle, and bone was less than 1% ID/g after injection 2 h, with fast blood clearance and low background interference. The uptake of [^{99m}Tc]Tc-EUKPG-TPPMS in the large intestine is particularly obvious, which may be related to the slightly higher lipophilicity. The kidney, as the dose-limiting organ for PSMA tracers,[21] is one of the important reference standards for screening promising tracers. Compared with [^{99m}Tc]Tc-EUKPG-TPPTS and [^{99m}Tc]Tc-EUKPG-TPPMS, [^{99m}Tc]Tc-EUKPG-EDDA showed the lowest renal uptake (3.51 ± 0.18 vs 4.08 ± 0.51 vs 12.83 ± 0.54% ID/g), and also shows the lowest uptake advantage in metabolic organs such as the liver and spleen. Compared to the other two coligands, EDDA has great potential in reducing uptake by nontarget organs, which may be related to its lower lipophilicity, in addition to its inherent advantages in molecular structure. The kidney is also one of the organs with high PSMA expression.[31] By preinjection of the blocker 2-PMPA, the uptake of [^{99m}Tc]Tc-EUKPG-EDDA in the kidney was significantly reduced, and the blocking rate (BR) was as high as 65%, demonstrating high specificity for PSMA. Therefore, [^{99m}Tc]Tc-EUKPG-EDDA enters follow-up research as a promising tracer.

The uptake of [^{99m}Tc]Tc-EUKPG-EDDA in cells was positively correlated with PSMA expression, and was reduced by 74% in PC3 (PSMA−) cells compared with the uptake in 22Rv1 (PSMA+) cells. At the same time, in the presence of the blocker 2-PMPA (1 μM), the inhibition group had only 16% uptake compared with the blank group, and the BR was as high as 84%. In addition, the effects of different concentrations (3−500 nM) of blockers on the cellular uptake of [^{99m}Tc]Tc-EUKPG-EDDA were investigated. It is gratifying that its uptake is inversely proportional to the concentration of the blocker, and the tracer and the blocker show an obvious competitive uptake relationship. Both differential and competitive uptake indicate that [^{99m}Tc]Tc-EUKPG-EDDA has good targeting to PSMA. At the same time, the affinity of [^{99m}Tc]Tc-EUKPG-EDDA for PSMA was measured at the nanomolar level (K_d = 23.33 nM) in 22Rv1 cells, further verifying its high affinity for PSMA. We theoretically verified the affinity performance of Tc-EUKPG-EDDA by MD simulation. The RMSD of the protein backbone and protein−ligand indicated stability within the entire 50 ns simulation step. The obvious fluctuation of the ligand residues allowed extensive hydrogen bonds and hydrophobic interactions to form in the active cavity of the protein. Through the MMPBSA energy decomposition analysis, the hydrogen bond formed by ARG534 and carbonyl oxygen (EUK) and the salt bridge formed by GLU542 and secondary amine hydrogen (EDDA) may be important for maintaining the stable structure of the protein−ligand, and are also the main influencing residues of MM, PB and SA energy. The total energy of the entire simulation system dG = −36.034 kJ/mol. The theoretical affinity between the ligand and the protein calculated by the total energy is at the nanomolar level (approximately 100 nM). It is exciting that it is highly consistent with the affinity level measured in the experiment, which proves the rationality of the kinetic simulation analysis results and provides a reliable theoretical model for the subsequent design of radiopharmaceuticals for PSMA targets.

22Rv1 mice model is widely used for the performance evaluation of PSMA tracers.[14,31] The biodistribution of [^{99m}Tc]Tc-EUKPG-EDDA in 22Rv1 tumor-bearing mice showed that its uptake in nontarget organs was less than 1% ID/g. The kidney was still the highest uptake organ (14.04 ± 0.23% ID/g), which was consistent with that observed in Kunming mice, followed by the tumor (1.07 ± 0.12% ID/g). The low background uptake gave it good TBRs, with T/B being 7.4 and T/M being 12.65. One of the design strategies in this study is introducing PG chains to reduce renal uptake. Compared with the previously reported HYNIC-derived tracers [^{99m}Tc]Tc-HYNIC-ALUG[19] (hexane derivative as the linker) and [^{99m}Tc]Tc-M2[31] (triazole ring derivative as the linker) (Figure S2), [^{99m}Tc]Tc-EUKPG-EDDA significantly reduced renal uptake (197.50 ± 7.1 vs 72.66 ± 4.40 vs 14.04 ± 0.23% ID/g, after injection 2 h), demonstrating the potential of PG linkers in reducing renal uptake, and the biodistribution results obtained in tumor-bearing mice supported the original goals of this study.

SPECT/CT imaging of [^{99m}Tc]Tc-EUKPG-EDDA in the 22Rv1 mice model showed that it is feasible for the diagnosis of prostate cancer. The tumor can be clearly located at all time points, and there is a high uptake in the kidney which is consistent with the biodistribution results. Under the condition of preinjection of the blocking agent 2-PMPA, the uptake of both the tumor and the kidney can be effectively inhibited. At the same time, in PC3 (PSMA-) mice model, the tumor uptake is negligible, and there is still a high uptake level in the kidney. SPECT/CT imaging in two models with differential expression of PSMA further verified the high specificity of [^{99m}Tc]Tc-EUKPG-EDDA for PSMA, indicating that it is a promising PSMA imaging agent for the diagnosis of prostate cancer.

CONCLUSIONS

In this study, we designed and synthesized a PSMA-targeted labeling precursor EUKPG, and three ^{99m}Tc-labeled radiotracers were prepared through different coligand combinations. They all showed good stability and hydrophilic *in vitro*. The differential and competitive uptake of [^{99m}Tc]Tc-EUKPG-EDDA in cells demonstrates its high specificity for PSMA, while significantly reducing the uptake in the kidneys. The low uptake and rapid clearance in nontarget organs make it have high TBRs. [^{99m}Tc]Tc-EUKPG-EDDA showed clear and accurate tumor location in SPECT/CT imaging, indicating that it is a promising candidate for PSMA-targeted tumor imaging agent.

https://doi.org/10.1021/acs.molpharmaceut.4c00799
Mol. Pharmaceutics 2024, 21, 5305−5314

■ ASSOCIATED CONTENT

Supporting Information

The Supporting Information is available free of charge at https://pubs.acs.org/doi/10.1021/acs.molpharmaceut.4c00799.

^{1}H NMR, MS spectra, biodistribution, and micro-SPECT/CT images in 22Rv1 and PC3 mice model (PDF)

■ AUTHOR INFORMATION

Corresponding Authors

Qing Ruan − *Key Laboratory of Radiopharmaceuticals of the Ministry of Education, College of Chemistry, NMPA Key Laboratory for Research and Evaluation of Radiopharmaceuticals (National Medical Products Administration) and Key Laboratory of Beam Technology of the Ministry of Education, College of Physics and Astronomy, Beijing Normal University, Beijing 100875, P. R. China;* orcid.org/0000-0003-1586-1682; Email: ruanqing0926@163.com

Junbo Zhang − *Key Laboratory of Radiopharmaceuticals of the Ministry of Education, College of Chemistry, NMPA Key Laboratory for Research and Evaluation of Radiopharmaceuticals (National Medical Products Administration), Beijing Normal University, Beijing 100875, P. R. China;* orcid.org/0000-0003-3549-6483; Email: zhjunbo@bnu.edu.cn

Authors

Zuojie Li − *Key Laboratory of Radiopharmaceuticals of the Ministry of Education, College of Chemistry, NMPA Key Laboratory for Research and Evaluation of Radiopharmaceuticals (National Medical Products Administration), Beijing Normal University, Beijing 100875, P. R. China*

Yuhao Jiang − *Key Laboratory of Radiopharmaceuticals of the Ministry of Education, College of Chemistry, NMPA Key Laboratory for Research and Evaluation of Radiopharmaceuticals (National Medical Products Administration) and Key Laboratory of Beam Technology of the Ministry of Education, College of Physics and Astronomy, Beijing Normal University, Beijing 100875, P. R. China*

Guangxing Yin − *Key Laboratory of Radiopharmaceuticals of the Ministry of Education, College of Chemistry, NMPA Key Laboratory for Research and Evaluation of Radiopharmaceuticals (National Medical Products Administration), Beijing Normal University, Beijing 100875, P. R. China*

Peiwen Han − *Key Laboratory of Radiopharmaceuticals of the Ministry of Education, College of Chemistry, NMPA Key Laboratory for Research and Evaluation of Radiopharmaceuticals (National Medical Products Administration), Beijing Normal University, Beijing 100875, P. R. China*

Xiaojiang Duan − *Department of Nuclear Medicine, Peking University First Hospital, Beijing 100034, P. R. China*

Complete contact information is available at: https://pubs.acs.org/10.1021/acs.molpharmaceut.4c00799

Notes

The authors declare no competing financial interest.

■ ACKNOWLEDGMENTS

This work was financially supported, in part, by the National Natural Science Foundation of China (22076013, 22276015), the Beijing Natural Science Foundation (2232010), and the Beijing Nova Program (20230484470).

■ ABBREVIATIONS

BR, blocking rate; DCM, dichloromethane; DMF, dimethylformamide; EDDA, ethylenediaminediacetic acid; EUK, glu-urea-lysine; FAP, fibroblast activation protein; tricine, trimethylglycine; HATU, tetramethylurea hexafluorophosphate; HYNIC, hydrazinonicotinamide; IA, injected activity; MeOH, methanol; MM, molecular mechanics energy; MMPBSA, molecular mechanics Poisson−Boltzmann surface area; MS, mass spectra; NMR, nuclear magnetic resonance; PB, polarized solvation energy; PBS, phosphate buffered saline; PDB, protein data bank; PET, positron emission tomography; PG, $_D$Pro-Gly; PSA, prostate-specific antigen; PSMA, prostate-specific membrane antigen; RCP, radiochemical purity; R-HPLC, radioactive high-performance liquid chromatography; RMSD, root-mean-square deviation; RMSF, root-mean-square fluctuation; RT, retention times; SA, nonpolar solvation energy; SB, specific binding; SD, standard deviation; SPECT, single photon emission computed tomography; TBRs, tumor-to-background ratios; TEA, triethylamine; TFA, trifluoroacetic acid; TLC, thin-layer chromatography; TPPTS, triphenylphosphine trisulfonate; TPPMS, diphenylphosphine benzene-3-sulfonate

■ REFERENCES

(1) Lawhn-Heath, C.; Salavati, A.; Behr, S. C.; Rowe, S. P.; Calais, J.; Fendler, W. P.; Eiber, M.; Emmett, L.; Hofman, M. S.; Hope, T. A. Prostate-Specific Membrane Antigen PET in Prostate Cancer. *Radiology* **2021**, *299* (2), 248−260.

(2) Spatz, S.; Tolkach, Y.; Jung, K.; Stephan, C.; Busch, J.; Ralla, B.; Rabien, A.; Feldmann, G.; Brossart, P.; Bundschuh, R. A.; et al. Comprehensive Evaluation of Prostate Specific Membrane Antigen Expression in the Vasculature of Renal Tumors: Implications for Imaging Studies and Prognostic Role. *J. Urol* **2018**, *199* (2), 370−377.

(3) Ahmad, A.; Schmidt, L. H.; Heitkötter, B.; Schulze, A. B.; Schliemann, C.; Steinestel, K.; Trautmann, M.; Marra, A.; Hillejan, L.; Mohr, M.; et al. Prostate Specific Membrane Antigen (PSMA) Expression in Non-Small Cell Lung Cancer. *PLoS One* **2017**, *12* (10), No. e0186280.

(4) Uijen, M. J. M.; Derks, Y. H. W.; Merkx, R. I. J.; Schilham, M. G. M.; Roosen, J.; Privé, B. M.; van Lith, S. A. M.; van Herpen, C. M. L.; Gotthardt, M.; Heskamp, S.; et al. PSMA Radioligand Therapy for Solid Tumors Other Than Prostate Cancer: Background, Opportunities, Challenges, and First Clinical Reports. *Eur. J. Nucl. Med. Mol. Imaging* **2021**, *48* (13), 4350−4368.

(5) Murphy, D. G.; Sathianathen, N.; Hofman, M. S.; Azad, A.; Lawrentschuk, N. Where to Next for Theranostics in Prostate Cancer? *Eur. Urol Oncol* **2019**, *2* (2), 163−165.

(6) Sgouros, G.; Bodei, L.; McDevitt, M. R.; Nedrow, J. R. Radiopharmaceutical Therapy in Cancer: Clinical Advances and Challenges. *Nat. Rev. Drug Discov* **2020**, *19* (9), 589−608.

(7) Cui, X. Y.; Liu, Y.; Wang, C.; Wen, Z.; Li, Y.; Tang, H.; Diwu, J.; Yang, Y.; Cui, M.; Liu, Z. China's Radiopharmaceuticals on Expressway: 2014−2021. *Radiol Acta* **2022**, *110* (6−9), 765−784.

(8) Zhang, Z.; Zhu, Z.; Yang, D.; Fan, W.; Wang, J.; Li, X.; Chen, X.; Wang, Q.; Song, X. Preparation and Affinity Identification of Glutamic Acid-Urea Small Molecule Analogs in Prostate Cancer. *Oncol Lett.* **2016**, *12* (2), 1001−1006.

(9) Corpetti, M.; Müller, C.; Beltran, H.; de Bono, J.; Theurillat, J. P. Prostate-Specific Membrane Antigen−Targeted Therapies for Pros-

tate Cancer: Towards Improving Therapeutic Outcomes. *Eur. Urol* **2024**, *85*, 193−204.
(10) Wester, H. J.; Schottelius, M. PSMA-Targeted Radiopharmaceuticals for Imaging and Therapy. *Semin Nucl. Med.* **2019**, *49* (4), 302−312.
(11) Duatti, A. Review on ^{99m}Tc Radiopharmaceuticals with Emphasis on New Advancements. *Nucl. Med. Biol.* **2021**, *92*, 202−216.
(12) Crisan, G.; Moldovean-Cioroianu, N. S.; Timaru, D. G.; Andries, G.; Cainap, C.; Chis, V. Radiopharmaceuticals for PET and SPECT Imaging: A Literature Review over the Last Decade. *Int. J. Mol. Sci.* **2022**, *23* (9), 5023−5074.
(13) Neels, O. C.; Kopka, K.; Liolios, C.; Afshar-Oromieh, A. Radiolabeled PSMA Inhibitors. *Cancers* **2021**, *13* (24), 6255−6278.
(14) Brunello, S.; Salvarese, N.; Carpanese, D.; Gobbi, C.; Melendez-Alafort, L.; Bolzati, C. A Review on the Current State and Future Perspectives of [^{99m}Tc]Tc-Housed PSMA-i in Prostate Cancer. *Molecules* **2022**, *27* (9), 2617−2656.
(15) Fanti, S.; Minozzi, S.; Antoch, G.; Banks, I.; Briganti, A.; Carrio, I.; Chiti, A.; Clarke, N.; Eiber, M.; De Bono, J.; et al. Consensus on Molecular Imaging and Theranostics in Prostate Cancer. *Lancet Oncol* **2018**, *19* (12), e696−e708.
(16) Hillier, S. M.; Maresca, K. P.; Lu, G.; Merkin, R. D.; Marquis, J. C.; Zimmerman, C. N.; Eckelman, W. C.; Joyal, J. L.; Babich, J. W. ^{99m}Tc-Labeled Small-Molecule Inhibitors of Prostate-Specific Membrane Antigen for Molecular Imaging of Prostate Cancer. *J. Nucl. Med.* **2013**, *54* (8), 1369−1376.
(17) Robu, S.; Schottelius, M.; Eiber, M.; Maurer, T.; Gschwend, J.; Schwaiger, M.; Wester, H. J. PSMA -Preclinical Evaluation and First Patient Application of ^{99m}Tc- PSMA-I&S for SPECT Imaging and Radioguided Surgery in Prostate Cancer. *J. Nucl. Med.* **2017**, *58* (2), 235−242.
(18) Ferro-Flores, G.; Luna-Gutiérrez, M.; Ocampo-García, B.; Santos-Cuevas, C.; Azorín-Vega, E.; Jiménez-Mancilla, N.; Orocio-Rodríguez, E.; Davanzo, J.; García-Pérez, F. O. Clinical Translation of a PSMA Inhibitor for ^{99m}Tc-Based SPECT. *Nucl. Med. Biol.* **2017**, *48*, 36−44.
(19) Xu, X.; Zhang, J.; Hu, S.; He, S.; Bao, X.; Ma, G.; Luo, J.; Cheng, J.; Zhang, Y. ^{99m}Tc-Labeling and Evaluation of a Hynic Modified Small-Molecular Inhibitor of Prostate-Specific Membrane Antigen. *Nucl. Med. Biol.* **2017**, *48*, 69−75.
(20) Ćwikła, J. B.; Roslan, M.; Skoneczna, I.; Kempińska-Wróbel, M.; Maurin, M.; Rogowski, W.; Janota, B.; Szarowicz, A.; Garnuszek, P. Initial Experience of Clinical Use of [^{99m}Tc]Tc-PSMA-T4 in Patients with Prostate Cancer. A Pilot Study. *Pharmaceuticals* **2021**, *14* (11), 1107−1122.
(21) Sallam, M.; Nguyen, N.-T.; Sainsbury, F.; Kimizuka, N.; Muyldermans, S.; Benešová-Schäfer, M. PSMA-Targeted Radiotheranostics in Modern Nuclear Medicine: Then, Now, and What of the Future? *Theranostics* **2024**, *14* (8), 3043−3079.
(22) Mizuno, Y.; Kimura, K.; Onoe, S.; Shukuri, M.; Kuge, Y.; Akizawa, H. Influence of Linker Molecules in Hexavalent RGD Peptides on Their Multivalent Interactions with Integrin $\alpha_v\beta_3$. *J. Med. Chem.* **2021**, *64* (21), 16008−16019.
(23) Ruan, Q.; Wang, Q. N.; Jiang, Y. H.; Feng, J. H.; Yin, G. X.; Zhang, J. B. Synthesis and Evaluation of ^{99m}Tc-Labeled FAP Inhibitors with Different Linkers for Imaging of Fibroblast Activation Proteins in Tumors. *J. Med. Chem.* **2023**, *66* (7), 4952−4960.
(24) Ruan, Q.; Ding, D. J.; Diao, L. A.; Feng, J. H.; Yin, G. X.; Jiang, Y. H.; Wang, Q. N.; Han, P. W.; Jiang, J. Y.; Zhang, J. B. Synthesis and Preclinical Evaluation of Novel ^{99m}Tc-Labeled FAPI-46 Derivatives with Significant Tumor Uptake and Improved Tumor-to-Nontarget Ratios. *J. Med. Chem.* **2024**, *67* (4), 3190−3202.
(25) Shi, J.; Liu, S. Clinical Application of ^{99m}Tc-Labeled Peptides for Tumor Imaging: Current Status and Future Directions. *iRADIOLOGY* **2024**, *2* (1), 17−34.
(26) Papagiannopoulou, D. Technetium-99m Radiochemistry for Pharmaceutical Applications. *J. Labelled Comp Radiopharm* **2017**, *60* (11), 502−520.
(27) Liu, S.; Edwards, D. S.; Harris, A. R. A Novel Ternary Ligand System for ^{99m}Tc Labeling of Hydrazino Nicotinamide Modified Biologically Active. *Bioconjug Chem.* **1998**, *9*, 583−595.
(28) Torabizadeh, S. A.; Hosseinimehr, S. The Influence of Co-Ligands on Improving Tumor Targeting of ^{99m}Tc-HYNIC Conjugated Peptides. *Mini Rev. Med. Chem.* **2016**, *17* (2), 86−94.
(29) Ahmed, N.; Zia, M. Diagnostic Modalities and Radiopharmaceuticals with Particular Importance of Technetium-99m (^{99m}Tc). *Chin J. Acad. Radiol* **2023**, *6* (4), 143−159.
(30) Gan, Q. Q.; Song, X. Q.; Zhang, X. R.; Zhang, J. B. Preparation and Evaluation of ^{99m}Tc-Labeled HYNIC-Palbociclib Analogs for Cyclin-Dependent Kinase 4/6-Positive Tumor Imaging. *Eur. J. Med. Chem.* **2020**, *188*, 112032−112041.
(31) Xiao, D.; Han, P. W.; Jiang, Y. H.; Duan, X. J.; Ruan, Q.; Zhang, Z. B.; Chen, X. L.; Zhang, J. B. Preparation, Biological Evaluation, and First-in-Human Single-Photon Emission Computed Tomography (SPECT) Study of ^{99m}Tc-Labeled Prostate-Specific Membrane Antigen (PSMA)-Targeted Radiotracers Containing Triazole with Reduced Kidneys Accumulation. *ACS Pharmacol Transl Sci.* **2024**, *7* (5), 1335−1347.

https://doi.org/10.1021/acs.molpharmaceut.4c00799
Mol. Pharmaceutics 2024, 21, 5305−5314